

# Bayesian Neural Network Detector for an Orthogonal Time Frequency Space Modulation

Alva Kosasih\*, Xinwei Qu\*, Wibowo Hardjawana\*, Chentao Yue\*, and Branka Vucetic\*

\*Centre of Excellence in Telecommunications, University of Sydney, Sydney, Australia.

{alva.kosasih,wibowo.hardjawana,chentao.yue,branka.vucetic}@sydney.edu.au, xiqu4217@uni.sydney.edu.au.

**Abstract**—The orthogonal time frequency space (OTFS) modulation is proposed for beyond 5G wireless systems to deal with high mobility communications. The existing low complexity OTFS detectors’ performance is suboptimal in rich scattering environments where there are a large number of moving reflectors that reflect the transmitted signal towards the receiver. In this paper, we propose an OTFS detector, referred to as the BPICNet OTFS detector that integrates NN, Bayesian inference, and parallel interference cancellation concepts. Simulation results show that the proposed detector outperforms the state-of-the-art.

**Index Terms**—OTFS, neural network, interference cancellation, detection, mobile cellular networks.

## I. INTRODUCTION

Beyond 5G wireless system enables high-speed communications which involve unmanned aerial vehicles, trains, and autonomous cars [1]. As illustrated in Fig. 1, there is a high speed transmitter, several reflectors (i.e. the other moving vehicles/objects around the vicinity of the transmitter), and a base station receiver in an uplink scenario. The moving reflectors generate a high inter-carrier interference. This causes significant performance degradation in the current OFDM modulation [2], [3]. To address this issue, an orthogonal time frequency space (OTFS) modulation that multiplexes the information symbols in the delay-Doppler (DD) domain was proposed in [4]. The OTFS performance highly depends on its symbol detector at the receivers. To date, there are many works on OTFS symbol detectors. They can be categorised into two groups i.e., classical [2], [5]–[9] and neural-network (NN) [10], [11] based OTFS detectors.

A classical minimum-mean-square-error (MMSE) OTFS detector [5] provides a low complexity but demonstrating a suboptimal performance. A classical iterative message passing (MP) detector for OTFS systems [2] performs much better than the MMSE OTFS detector, where the interference is approximated using Gaussian functions. A variational Bayes (VB) OTFS detector has also been considered in [12] to improve the convergence of the MP OTFS detector. Unfortunately, their performance degrades significantly when the number of moving reflectors rises, referred to as a rich scattering environment. To achieve excellent performance under a rich scattering environment, the expectation propagation (EP) [8] OTFS detectors have been proposed. However, EP needs to perform matrix inverse operation/approximation in each iteration, resulting in a high complexity. To avoid the high complexity issue, a unitary approximate MP (UAMP) [7] and a Bayesian parallel interference cancellation (BPIC) [9] OTFS detectors were proposed. The UAMP applies singular value decomposition (SVD) on the OTFS channel matrix, transforms

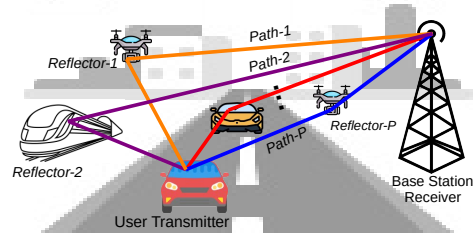


Fig. 1: High mobility environment

the received signal using the unitary matrix, and then performs the AMP scheme based on the transformed received signal to yield the symbol estimates. The BPIC estimates the symbols by iteratively mitigating the interference from the received signal in a parallel manner. The UAMP and BPIC demonstrate similar performance. However, there exists a performance gap between UAMP and BPIC with EP.

The second category of OTFS detectors, the NN based OTFS detectors have a better detection performance compared to the classical OTFS detectors. In [10], [11], the NNs are trained using simulated data consisting of the received signals and transmitted symbols to approximate the detection mapping function from the received signals to the transmitted symbol estimates. Unfortunately, the numbers of trainable NN parameters in both NN detectors are very large. This leads to high complexity and causes the parameters difficult to be optimized. A model-driven NN technique that introduces a few trainable NN parameters for classical iterative algorithms has been proposed in [13]–[15]. The OAMPNet [13] and the EPANet [14] add at most four NN parameters in each iteration of the orthogonal AMP (OAMP) and approximated EP detectors, respectively. However, they suffer from high complexity since they perform matrix inverse operations/approximations in every iteration. A model-driven NN detector named MMNet in [15] can achieve at par OAMPNet performance without performing matrix inverse operations. However, it requires a large number of additional NN parameters compared to the OAMPNet and EPANet, and thus its complexity is high. Note that all the above model-driven NN detectors are implemented in multiple-input multiple-output systems. To the best of our knowledge, there is no prior work on the model-driven NN detectors in the OTFS systems.

In this paper, we propose a low complexity NN based OTFS detector that can achieve a high detection performance under rich scattering environments. This is realized by integrating the BPIC and NN which we refer to as the BPIC Network

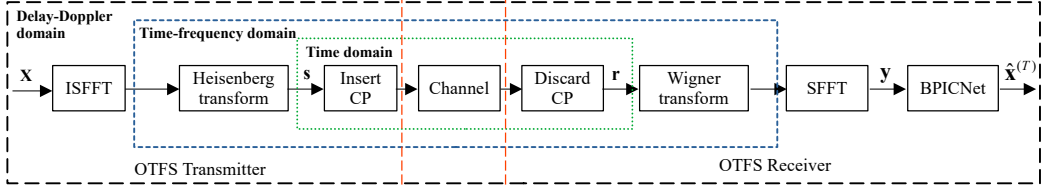


Fig. 2: The system model of OTFS modulation scheme

(BPICNet) detector. The original BPIC consists of three modules [16], namely: 1) the Bayesian symbol observation (BSO) module which employs a parallel interference cancellation (PIC) scheme to calculate the mean and variance of the transmitted symbols; 2) the Bayesian symbol estimate (BSE) module which calculates the soft symbol estimates based on the BSO outputs; 3) the decision statistic combining (DSC) module which weights the soft symbol estimates and their variance in the previous and current iterations. We develop the BPICNet by replacing the linear function<sup>1</sup> in the standard NN's neurons with modified BPIC functions, at each layer. These functions except the one in the BSE are treated as neurons where in each of the neurons there is a tunable parameter, referred to as the NN parameter. More specifically, two neurons are employed in the BSO while a neuron is employed in the DSC. The Bayesian symbol estimate (BSE) block contains a function calculating the soft symbol estimates and variances based on the Bayesian inference.

The main contribution of this paper is the first development of an OTFS detector that integrates NN, Bayesian inference, and PIC concepts. This results in a significant detection improvement as compared to its predecessor, BPIC detector [9], as well as the other low complexity OTFS detectors [2], [5]–[7]. Furthermore, unlike the state-of-the-art NN based OTFS detectors [10], [11] which optimize a large number of NN parameters, the BPICNet OTFS detector employs only three NN parameters in each layer and thus the parameters are much easier to be optimized.

**Notations:**  $a$ ,  $\mathbf{a}$  and  $\mathbf{A}$  denote scalar, vector, and matrix respectively.  $\mathbb{C}^{M \times N}$  denotes the set of  $M \times N$  dimensional complex matrices. We use  $\mathbf{I}_N$ ,  $\mathbf{F}_N$ , and  $\mathbf{F}_N^H$  to represent an  $N$ -dimensional identity matrix,  $N$ -points discrete Fourier Transform (DFT) matrix, and  $N$ -points inverse discrete Fourier transform (IDFT) matrix.  $(\cdot)^T$  represent the transpose operation. We define  $\mathbf{a} = \text{vec}(\mathbf{A})$  as the column-wise vectorization of matrix  $\mathbf{A}$  and its inverse operation  $\mathbf{A} = \text{vec}^{-1}(\mathbf{a})$ . The Kronecker product is denoted as  $\otimes$ . The Euclidean distance of vector  $\mathbf{x}$  is denoted as  $\|\mathbf{x}\|$ . We use  $\mathcal{N}(x; \mu, \sigma)$  to express a single variate Gaussian distribution of a random variable  $x$  where  $\mu$  is the mean and  $\sigma$  is the variance.

## II. SYSTEM MODEL

We consider an OTFS system, illustrated in Fig. 2. The transmitter and receiver are equipped with a single antenna. The channel state information (CSI) is assumed to be known in the receiver side. Note that the OTFS system can be

<sup>1</sup>A standard NN linear function is  $\theta\mathcal{X} + b$ , where  $\theta$  is an NN parameter,  $\mathcal{X}$  is an input, and  $b$  is a bias parameter.

developed by applying the inverse symplectic finite Fourier transform (ISFFT) and SFFT blocks at the OFDM transmitter and receiver, respectively [4]. In the following, we explain the details of the OTFS transmitter, channel, and receiver.

### A. OTFS Transmitter

In the transmitter side, we map the information binary sequences into the  $M$ -ary quadrature amplitude modulation ( $M$ -QAM) symbols where the constellation is denoted as  $\Omega$ . The matrix of QAM symbols  $\mathbf{X} \in \mathbb{C}^{L \times K}$  are assigned in the DD domain discretized to an  $L \times K$  grid, where  $L$  and  $K$  are the numbers of subcarriers and OTFS subframes in an OTFS frame. The quantization steps of the delay and Doppler axes are  $1/(L\Delta f)$  and  $1/(KT_s)$ , respectively.  $\Delta f$  and  $T_s$  are the subcarrier spacing and duration of an OTFS subframe, respectively. We transform the matrix of symbols  $\mathbf{X}$  from the DD domain into the time-frequency (TF) domain by using the ISFFT, as described in Fig. 2. The ISFFT is performed by applying  $L$ -points DFT to the columns and  $K$ -points IDFT to the rows of  $\mathbf{X}$  [17] i.e.,  $\mathbf{F}_L \mathbf{X} \mathbf{F}_K^H$ , where  $\mathbf{F}_L \in \mathbb{C}^{L \times L}$  and  $\mathbf{F}_K^H \in \mathbb{C}^{K \times K}$  are the DFT and IDFT matrices<sup>2</sup>, respectively. The TF domain is discretized to an  $L \times K$  grid with uniform intervals  $\Delta f$  (Hz) and  $T_s = 1/\Delta f$  (seconds) in frequency and time axes. Therefore, an OTFS frame occupies a bandwidth of  $L\Delta f$  and a duration of  $KT_s$ . A Heisenberg transform, consisting of an  $L$ -points IDFT and pulse shaping waveform, is then applied to generate the time-domain transmitted signal  $\mathbf{G}_{\text{tx}} \mathbf{F}_L^H (\mathbf{F}_L \mathbf{X} \mathbf{F}_K^H)$ , where  $\mathbf{G}_{\text{tx}} = \mathbf{I}_L$  for a rectangular waveform [17] with a duration of  $T_s$ . The transmitted signal is rewritten in a vector form as

$$\mathbf{s} = \text{vec}(\mathbf{I}_L \mathbf{X} \mathbf{F}_K^H) = (\mathbf{F}_K^H \otimes \mathbf{I}_L) \mathbf{x}, \quad \mathbf{x} = \text{vec}(\mathbf{X}), \quad (1)$$

obtained by using the Kronecker product rule<sup>3</sup>. We consider the OTFS model as in [17], where the cyclic prefix (CP) is inserted only at the beginning of the OTFS frame. For each OTFS frame, the time duration after adding CP is  $KT_s + N_{\text{cp}} \frac{T_s}{L}$ , where  $N_{\text{cp}}$  is equal to the index of the maximum delay.

### B. OTFS Wireless Channel

The OTFS wireless channel is a time-varying multipath channel, represented by the impulse responses in the DD domain,  $h(\tau, v) = \sum_{i=1}^P h_i \delta(\tau - \tau_i) \delta(v - v_i)$ , where  $\delta(\cdot)$

<sup>2</sup>The  $(p, q)$ -th entries of the  $N$ -points DFT and its inverse are  $(\frac{1}{\sqrt{N}} e^{-j2\pi(p-1)(q-1)/N})$  and  $(\frac{1}{\sqrt{N}} e^{j2\pi(p-1)(q-1)/N})$ ,  $p, q = 1, \dots, N$ , respectively.

<sup>3</sup>A matrix multiplication is often expressed by using vectorization with the Kronecker product. That is,  $\text{vec}(ABC) = (C^T \otimes A) \text{vec}(B)$

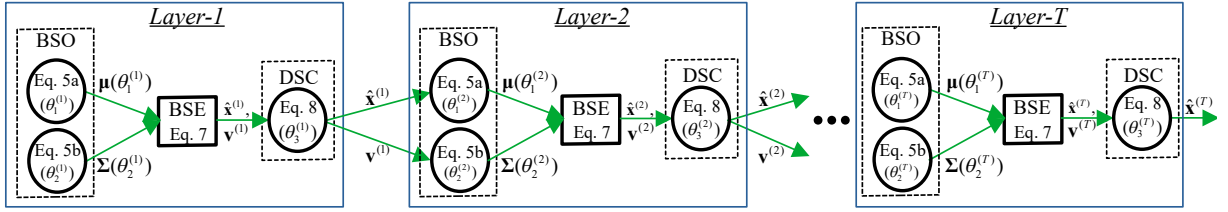


Fig. 3: The BPICNet OTFS detector with  $\theta_1^{(t)}, \theta_2^{(t)}$ , and  $\theta_3^{(t)}, t \in \{1, \dots, T\}$ , as the NN parameters

is the Dirac delta function,  $h_i \sim \mathcal{N}(0, 1/P)$  denotes the  $i$ -th path gain,  $P$  is the number of propagation paths, and each path is associated with a moving reflector as described in Fig. 1. The paths have different delay ( $\tau_i$ ) and/or Doppler ( $v_i$ ) characteristics. The delay and Doppler shifts are given as  $\tau_i = l_i \frac{T_s}{L}$  and  $v_i = (k_i + \kappa_i) \frac{\Delta f}{K}$ , respectively. The integers  $l_i \in [0, l_{\max}]$  and  $k_i \in [-k_{\max}, k_{\max}]$  denote the indices of the delay and Doppler shift in  $i$ -th path, where  $l_{\max} \leq L - 1$  and  $k_{\max} \leq \lfloor \frac{K}{2} \rfloor$  are the indices of the maximum delay and Doppler shift among all channel paths. The fractional Doppler,  $-0.5 < \kappa_i \leq 0.5$ ,  $\kappa_i \in \mathbb{R}$ , is set as  $\kappa_i = 0$ . This means we do not consider fractional Doppler shifts in this work and leave this for future work. The maximum number of paths in OTFS systems is  $(2k_{\max} + 1) \times l_{\max}$ .

### C. OTFS Receiver

We discard the CP from a received OTFS frame and thus the time domain received signal is given as [17]

$$\mathbf{r} = \mathbf{H}\mathbf{s} + \mathbf{w}, \quad (2)$$

where  $\mathbf{w}$  is the independent and identically distributed (i.i.d.) white Gaussian noise that follows  $\mathcal{N}(\mathbf{0}, \sigma^2 \mathbf{I}_{KL})$ ,  $\sigma^2$  is the variance of the noise,  $\mathbf{H} = \sum_{i=1}^P h_i \mathbf{I}_{KL}(l_i) \mathbf{\Delta}(k_i)$ ,  $\mathbf{I}_{KL}(l_i)$  denotes a  $KL \times KL$  matrix obtained by circularly left shifting the columns of the identity matrix by  $l_i$ ,  $\mathbf{\Delta}(k_i) = \text{diag} \left[ e^{\frac{j2\pi k_i(0)}{KL}}, e^{\frac{j2\pi k_i(1)}{KL}}, \dots, e^{\frac{j2\pi k_i(KL-1)}{KL}} \right]$  is a  $KL \times KL$  Doppler shift diagonal matrix, and  $\text{diag}(\cdot)$  denotes a diagonalization operation on a vector. As shown in Fig. 2, the received signal in the TF domain is obtained by applying the Wigner transform [17], that consists of an  $L$ -points DFT and a pulse shaping waveform with a duration of  $T_s$ . The TF domain received signal is  $\mathbf{F}_L \mathbf{G}_{\text{rx}} \mathbf{R}$ , where  $\mathbf{R} = \text{vec}^{-1}(\mathbf{r})$  and  $\mathbf{G}_{\text{rx}} = \mathbf{I}_L$  in the case of a rectangular waveform. A symplectic finite Fourier transform (SFFT) is then performed by applying  $L$ -points IDFT to the columns and an  $K$ -points IDFT to the rows of the TF domain received signal, expressed as  $\mathbf{F}_L^H (\mathbf{F}_L \mathbf{I}_L \mathbf{R}) \mathbf{F}_K = \mathbf{I}_L \mathbf{R} \mathbf{F}_K$ , which can be vectorized as

$$\mathbf{y} = \text{vec}(\mathbf{I}_L \mathbf{R} \mathbf{F}_K) = (\mathbf{F}_K \otimes \mathbf{I}_L) \mathbf{r}. \quad (3)$$

Substituting (1) into (2) and (3) gives us

$$\mathbf{y} = \mathbf{H}_{\text{eff}} \mathbf{x} + \tilde{\mathbf{w}}, \quad (4)$$

where  $\mathbf{H}_{\text{eff}} = (\mathbf{F}_K \otimes \mathbf{I}_L) \mathbf{H} (\mathbf{F}_K^H \otimes \mathbf{I}_L)$  and  $\tilde{\mathbf{w}} = (\mathbf{F}_K \otimes \mathbf{I}_L) \mathbf{w}$  denote the effective channel and noise in the DD domain, respectively. Note that  $\tilde{\mathbf{w}}$  is an i.i.d. Gaussian noise, since  $\mathbf{F}_K \otimes \mathbf{G}_{\text{rx}}$  is a unitary orthogonal matrix [4], [17]. The

complex-valued model in (4) can be transformed into an equivalent real-valued model, as explained in [18]. To this end we consider the equivalent real-valued model of (4) and keep the notations the same to make them uncluttered.

### III. BPICNET OTFS DETECTOR

In this section, we describe the development of the BPICNet detector for an OTFS system. There are  $T$  layers, where in each layer there are three neurons represented by the circles and a BSE block, as illustrated in Fig. 3. Since the BPICNet embeds the BPIC into NN, it can be described by the three BPIC modules i.e., the BSO, BSE, and DSC modules. We omit the subscript eff for notational simplicity.

#### A. Bayesian Symbol Observation (BSO)

The posterior probability distribution of the transmitted symbols  $\mathbf{x} = [x_1, \dots, x_q, \dots, x_{KL}]$  in (1) given the received signal  $\mathbf{y}$  and channel matrix  $\mathbf{H}$  in (4) can be approximated by using a product of independent Gaussian functions as  $p(\mathbf{x}|\mathbf{y}) \approx \prod_{q=1}^{KL} \mathcal{N}(x_q : \mu_q(\theta_1^{(t)}), \Sigma_q(\theta_2^{(t)}))$  [16].  $\mu_q(\theta_1^{(t)})$  and  $\Sigma_q(\theta_2^{(t)})$  are the mean and variance of the  $q$ -th Gaussian function of  $x_q$  in  $t$ -th layer which can be obtained from the matched filter based PIC scheme, given as

$$\mu_q(\theta_1^{(t)}) = \hat{x}_q^{(t-1)} + \theta_1^{(t)} \frac{\mathbf{h}_q^\top}{\|\mathbf{h}_q\|^2} (\mathbf{y} - \mathbf{H} \hat{\mathbf{x}}^{(t-1)}), \quad (5a)$$

$$\Sigma_q(\theta_2^{(t)}) = \frac{\theta_2^{(t)}}{(\mathbf{h}_q^\top \mathbf{h}_q)^2} \left( \sum_{\substack{j=1 \\ j \neq q}}^{KL} (\mathbf{h}_q^\top \mathbf{h}_j)^2 v_j^{(t-1)} + (\mathbf{h}_q^\top \mathbf{h}_q) \sigma^2 \right). \quad (5b)$$

$\mathbf{h}_q$  is the  $q$ -th column of matrix  $\mathbf{H}$ ,  $\hat{\mathbf{x}}^{(t-1)}$  is a vector of symbol estimates in layer  $t-1$ ,  $v_j^{(t-1)}$  is the  $j$ -th element in a vector variance of symbol estimates  $\mathbf{v}^{(t-1)}$ ,  $\theta_1^{(t)}$  is an NN parameter used to adjust the residual error of the BSO symbol estimates in layer  $t$ , and  $\theta_2^{(t)}$  is an NN parameter used to weight the BSO variance in layer  $t$ . Note that we use the MMSE scheme to produce the initial value of the symbol estimates,

$$\hat{\mathbf{x}}^{(0)} = (\mathbf{H}^\top \mathbf{H} + \sigma^2 \mathbf{I}_{KL})^{-1} \mathbf{H}^\top \mathbf{y}. \quad (6)$$

The vectors  $\boldsymbol{\mu}(\theta_1^{(t)}) = [\mu_1(\theta_1^{(t)}), \dots, \mu_{KL}(\theta_1^{(t)})]^\top$  and  $\boldsymbol{\Sigma}(\theta_2^{(t)}) = [\Sigma_1(\theta_2^{(t)}), \dots, \Sigma_{KL}(\theta_2^{(t)})]^\top$  are then forwarded to the BSE module, as depicted in Fig. 3.

### B. Bayesian Symbol Estimator (BSE)

In the BSE module, we compute the Bayesian symbol estimates and their variances based on the outputs of the BSO module. The Bayesian symbol estimate and variance of the  $q$ -th transmitted symbol are respectively given as

$$\hat{x}_q^{(t)} = \mathbb{E} \left[ x_q \middle| \mu_q(\theta_1^{(t)}), \Sigma_q(\theta_2^{(t)}) \right] = \sum_{a \in \Omega} ap^{(t)}(x_q = a | \mathbf{y}), \quad (7a)$$

$$v_q^{(t)} = \mathbb{E} \left[ \left| x_q - \mathbb{E} \left[ x_q \middle| \mu_q(\theta_1^{(t)}), \Sigma_q(\theta_2^{(t)}) \right] \right|^2 \right], \quad (7b)$$

where  $p^{(t)}(x_q | \mathbf{y}) = \mathcal{N}(x_q : \mu_q(\theta_1^{(t)}), \Sigma_q(\theta_2^{(t)}))$  is obtained from the BSO module and it is normalized so that  $\sum_{a \in \Omega} p^{(t)}(x_q = a | \mathbf{y}) = 1$ . The output vectors of the BSE module,  $\hat{\mathbf{x}}^{(t)} = [\hat{x}_1^{(t)}, \dots, \hat{x}_{KL}^{(t)}]^\top$  and  $\mathbf{v}^{(t)} = [v_1^{(t)}, \dots, v_{KL}^{(t)}]^\top$  are then sent to the DSC module.

### C. Decision Statistics Combining (DSC)

In the DSC module, we linearly combine the symbol estimate and variance in the subsequent layers, i.e.,

$$\hat{x}_q^{(t)} \leftarrow (1 - \rho_q(\theta_3^{(t)})) \cdot \hat{x}_q^{(t-1)} + \rho_q(\theta_3^{(t)}) \cdot \hat{x}_q^{(t)}, \quad (8a)$$

$$v_q^{(t)} \leftarrow (1 - \rho_q(\theta_3^{(t)})) \cdot v_q^{(t-1)} + \rho_q(\theta_3^{(t)}) \cdot v_q^{(t)}, \quad (8b)$$

where  $\rho_q(\theta_3^{(t)}) \triangleq \frac{e_q^{(t-1)}}{e_q^{(t)} + e_q^{(t-1)}}$ ,  $e_q^{(t)} = \theta_3^{(t)} |\mathbf{h}_q^\top (\mathbf{y} - \mathbf{H}\hat{\mathbf{x}}^{(t)})|^2$ , and  $\theta_3^{(t)}$  is an NN parameter used to adjust the square error of the symbol estimates in layer- $t$ . Note that  $\theta_3^{(t)}$  allows the BPICNet to fine-tune the DSC coefficients and thus regulates the update portion of the symbol estimates and variances in each layer. The weighted symbol estimate and variance vectors,  $\hat{\mathbf{x}}^{(t)}$  and  $\mathbf{v}^{(t)}$ , are then fed back to the BSO module to proceed the computations in the next layer. The processes are repeated for  $T$  times as depicted in Fig. 3. The complete pseudo-code of the BPICNet OTFS detector is given in Algorithm 1.

---

#### Algorithm 1 The BPICNet OTFS detector

---

```

1: Input:  $\mathbf{y}, \mathbf{H}, \sigma^2, T$ 
2: for  $t = 1, \dots, T$  do
3:   if  $t = 1$  then
4:     Compute (6)
5:   end if
6:   The BSO Module:
7:     Compute (5a) to obtain  $\boldsymbol{\mu}(\theta_1^{(t)})$ 
8:     Compute (5b) to obtain  $\boldsymbol{\Sigma}(\theta_2^{(t)})$ 
9:   The BSE Module:
10:    Compute (7a) to obtain  $\hat{\mathbf{x}}^{(t)}$ 
11:    Compute (7b) to obtain  $\mathbf{v}^{(t)}$ 
12:   The DSC Module:
13:    Compute (8a) to obtain weighted  $\hat{\mathbf{x}}^{(t)}$ 
14:    Compute (8b) to obtain weighted  $\mathbf{v}^{(t)}$ 
15: end for
16: Output:  $\hat{\mathbf{x}}^{(T)} = [\hat{x}_1^{(T)}, \dots, \hat{x}_{KL}^{(T)}]^\top$ 

```

---

Table I: Computational complexity comparison

OTFS detector	Complexity	T	Numerical example $K = 7, L = 12, M = 4, P = 14, (\times 10^5)$
MP [2]	$\mathcal{O}((KL)^2 PMT)$	9	35.5622
UAMP [7]	$\mathcal{O}((KL)^3 + (KL)^2 T)$	9	6.56208
BPIC [9]	$\mathcal{O}((KL)^3 + (KL)^2 T)$	8	6.4915
BPICNet	$\mathcal{O}((KL)^3 + KL + (KL)^2 T)$	9	6.56208
EP [8]	$\mathcal{O}((KL)^3 T)$	5	29.6352

## IV. COMPLEXITY ANALYSIS

In this section, we analyze the complexity of the proposed BPICNet OTFS detector. Algorithm 1 specifies that the BPICNet performs matrix vector multiplications at each layer in (5), (7)-(8) and therefore the cost is  $\mathcal{O}((KL)^2 T)$  in terms of the number of multiplications. The matrix inverse operation, performed in (6) requires  $\mathcal{O}((KL)^3)$ . Note that the complexity of multiplying three NN parameters in each layer is small as its cost is only  $\mathcal{O}(KL)$ . As given in Table 1, the complexity of the BPICNet is around four times lower than the EP's complexity and similar to that of the BPIC and UAMP.

## V. SIMULATION RESULTS

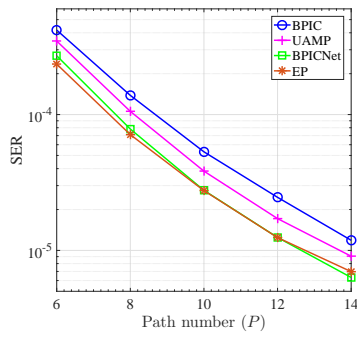
We first explain the training of the proposed detector and compare its performance with MP [2], UAMP [7], BPIC [9], and EP [8] OTFS detectors. We set  $T = 10, K = 7, \Delta f = 15\text{kHz}, k_{\max} = 3, \text{SNR} = 15\text{dB}$ , and employ 4-QAM modulation. The carrier frequency is set to  $f_c = 10\text{GHz}$ .

### A. Training of the BPICNet OTFS Detector

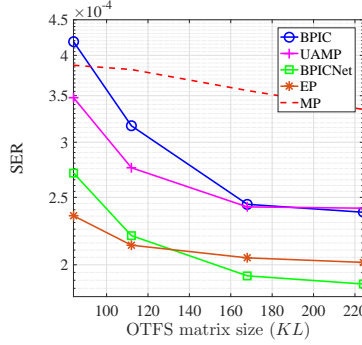
We implemented the BPICNet in PyTorch. The training was divided into 500 epochs. In each epoch, 40 batches of 256 samples were generated, where a sample includes realizations of  $\mathbf{x}_{\text{DD}}, \tilde{\mathbf{w}}$ , and  $\mathbf{H}_{\text{eff}}$  satisfying (4). In each batch, we randomly chose  $P \in \{6, \dots, 14\}$  while the SNR values are uniformly distributed in a certain range. Therefore, the BPICNet OTFS detector can be implemented in systems with dynamic changes in  $P$  without retraining. We used Adam optimizer with learning rate of 0.0001 and applied the learning rate scheduler (PyTorch ReduceLRonPlateau) to adjust the learning rate based on the validation loss, computed using additional 5000 samples in each epoch. In each batch, we calculated the average mean square error loss as

$$\text{Loss} = \frac{1}{256} \sum_{w=1}^{256} \sum_{q=1}^{KL} \left( x_{q,w} - \hat{x}_{q,w}^{(T)} \right)^2, \quad (9)$$

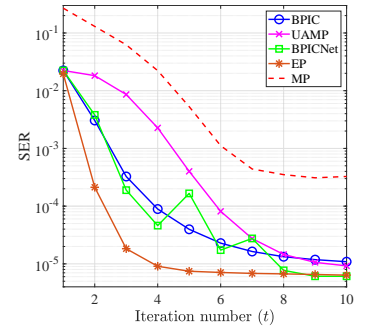
where  $w$  is the index of the training samples in each batch and  $\hat{x}_{q,w}^{(T)}$  refers to the final BPICNet symbol estimate of  $x_{q,w}$  obtained from the last  $T$ -th layer. The NN parameters i.e.,  $\theta_1^{(t)}, \theta_2^{(t)}$ , and  $\theta_3^{(t)}, t = 1, \dots, T$  were adjusted to minimize the loss in (9) using the backpropagation.



(a) SER vs number of paths,  $L = 12$ ,  $l_{\max} = 11$



(b) SER vs OTFS matrix size,  $P = 6$ ,  $l_{\max} = L - 1$



(c) SER vs iterations,  $P = 14$ ,  $L = 12$ ,  $l_{\max} = 11$

Fig. 4: The SER performance comparison

### B. SER Comparison

Fig. 4a demonstrates that the BPICNet OTFS detector significantly outperforms the other detectors except for the EP OTFS detector when the number of moving reflectors increases. The BPICNet achieves a similar SER performance to the EP with much lower complexity, as discussed in Section IV. Fig. 4b evaluates SER with respect to the OTFS matrix size. It is done by fixing  $K = 7$  while varying  $L \in \{12, 16, 24, 32\}$ . The result shows the outperformance of the proposed detector compared to the state-of-the-art. The BPICNet detector has a similar convergence rate as the standard BPIC and UAMP detectors, as illustrated in Fig. 4c. Nevertheless, the BPICNet assures a better SER performance

## VI. CONCLUSION

We proposed a BPICNet detector for an OTFS system. It achieved a high detection performance under rich scattering environment. Our simulation results showed that the BPICNet achieved a similar EP performance.

### ACKNOWLEDGMENT

This research was supported by the research training program stipend from The University of Sydney, Australian Research Council grant number DP210103410, and the ARC Laureate Fellowship grant number FL160100032.

### REFERENCES

- [1] N. Hashimoto, N. Osawa, K. Yamazaki, and S. Ibi. Channel estimation and equalization for CP-OFDM-based OTFS in fractional doppler channels. [Online]. Available: <https://arxiv.org/abs/2010.15396>
- [2] P. Raviteja, K. T. Phan, Y. Hong, and E. Viterbo, "Interference cancellation and iterative detection for orthogonal time frequency space modulation," *IEEE Trans. Wireless Commun.*, vol. 17, no. 10, pp. 6501–6515, August 2018.
- [3] Z. Wei, W. Yuan, S. Li, J. Yuan, G. Bharatula, R. Hadani, and L. Hanzo, "Orthogonal time-frequency space modulation: A promising next-generation waveform," *IEEE Wireless Commun.*, vol. 28, no. 4, pp. 136–144, Aug. 2021.
- [4] R. Hadani, S. Rakib, M. Tsatsanis, A. Monk, A. J. Goldsmith, A. F. Molisch, and R. Calderbank, "Orthogonal time frequency space modulation," in *Proc. IEEE Wireless Commun. and Netw. Conf. (WCNC)*, USA, March 2017, pp. 1–6.

- [5] P. Singh, A. Gupta, H. B. Mishra, and R. Budhiraja. Low-complexity ZF/MMSE receivers for MIMO-OTFS systems with imperfect CSI. [Online]. Available: <https://arxiv.org/abs/2010.04057>
- [6] L. Xiang, Y. Liu, L.-L. Yang, and L. Hanzo, "Gaussian approximate message passing detection of orthogonal time frequency space modulation," *IEEE Trans. Vehic. Technol.*, vol. 70, no. 10, pp. 10999–11004, Oct. 2021.
- [7] Z. Yuan, F. Liu, W. Yuan, Q. Guo, Z. Wang, and J. Yuan, "Iterative detection for orthogonal time frequency space modulation with unitary approximate message passing," *IEEE Trans. on Wireless Commun.*, vol. 21, no. 2, pp. 714–725, July 2022.
- [8] F. Long, K. Niu and J. Lin, "Low complexity block equalizer for OTFS based on expectation propagation," *IEEE Wireless Commun. Lett.*, vol. 11, no. 2, pp. 2514–2518, Feb. 2022.
- [9] X. Qu, A. Kosasih, W. Hardjawana, V. Onasis, and B. Vucetic, "Bayesian-based symbol detector for orthogonal time frequency space modulation systems," in *Proc. IEEE Int. Symp. Pers. Indoor Mob. Radio Commun. (PIMRC)*, Finland, Sept. 2021.
- [10] A. Naikoti and A. Chockalingam, "Low-complexity delay-Doppler symbol DNN for OTFS signal detection," in *Proc. IEEE Vehic. Technol. Conf. (VTC-Spring)*, Finland, Sept. 2021.
- [11] Y. K. Enku, B. Bai, F. Wan, C. U. Guyo, I. N. Tiba, C. Zhang, and S. Li, "Two-dimensional convolutional neural network-based signal detection for OTFS systems," *IEEE Wireless Commun. Lett.*, vol. 10, no. 11, pp. 2514–2518, Nov. 2021.
- [12] W. Yuan, Z. Wei, J. Yuan, and D. W. K. Ng, "A simple variational bayes detector for orthogonal time frequency space (otfs) modulation," *IEEE Trans. on Vehic. Technol.*, vol. 69, no. 7, pp. 7976–7980, July 2020.
- [13] H. He, C.-K. Wen, S. Jin, and G. Y. Li, "Model-Driven deep learning for MIMO detection," *IEEE Trans. Signal Process.*, vol. 68, pp. 1702–1715, Feb. 2020.
- [14] Y. Ge, X. Tan, Z. Ji, Z. Zhang, Y. Xiaohu, and C. Zhang, "Improving approximate expectation propagation massive mimo detector with deep learning," *IEEE Wireless Commun. Lett.*, vol. 10, no. 10, pp. 2145–2149, Oct. 2021.
- [15] M. Khani, M. Alizadeh, J. Hoydis and P. Fleming, "Adaptive neural signal detection for massive MIMO," *IEEE Trans. Wireless Commun.*, vol. 19, no. 8, pp. 5635–5648, Aug. 2020.
- [16] A. Kosasih, V. Miloslavskaya, W. Hardjawana, C. She, C. K. Wen and B. Vucetic, "A Bayesian receiver with improved complexity-reliability trade-off in massive MIMO systems," *IEEE Trans. Commun.*, vol. 69, no. 9, pp. 6251–6266, Sept. 2021.
- [17] P. Raviteja, Y. Hong, E. Viterbo, and E. Biglieri, "Practical pulse-shaping waveforms for reduced-cyclic-prefix OTFS," *IEEE Trans. on Vehic. Technol.*, vol. 68, no. 1, pp. 957–961, 2019.
- [18] J. Goldberger and A. Leshem, "A gaussian tree approximation for integer least-squares," in *Adv. Neural Inf. Process. Syst.*, vol. 22. Curran Associates, Inc., 2009.